

Semiclassical wave packet calculations on ion–molecule reactions: Studies on $B + (3P_u) + H_2$ reaction

Amrendra Vijay and G. D. Billing

Citation: *The Journal of Chemical Physics* **107**, 2974 (1997); doi: 10.1063/1.474655

View online: <http://dx.doi.org/10.1063/1.474655>

View Table of Contents: <http://scitation.aip.org/content/aip/journal/jcp/107/8?ver=pdfcov>

Published by the [AIP Publishing](#)

Articles you may be interested in

Time dependent quantum dynamics study of the $O + H_2 (v = 0, j = 0) \rightarrow OH + H$ ion-molecule reaction and isotopic variants (D_2, HD)

J. Chem. Phys. **125**, 164305 (2006); 10.1063/1.2359727

Exact quantum dynamics study of the $O + H_2 (v = 0, j = 0) \rightarrow OH + H$ ion-molecule reaction and comparison with quasiclassical trajectory calculations

J. Chem. Phys. **124**, 144301 (2006); 10.1063/1.2179429

Cross sections of the $O + H_2 \rightarrow OH + H$ ion-molecule reaction and isotopic variants (D_2, HD): Quasiclassical trajectory study and comparison with experiments

J. Chem. Phys. **123**, 174312 (2005); 10.1063/1.2098667

Interpolated potential energy surface and reaction dynamics for $O(3P) + H_3(1A1')$ and $OH(3\Sigma^-) + H_2(1\Sigma_g^+)$

J. Chem. Phys. **111**, 6322 (1999); 10.1063/1.479937

Theoretical study of the reactions of $Ar + H_2$ and $Ar + HD$ using the trajectory surface hopping method

J. Chem. Phys. **109**, 4815 (1998); 10.1063/1.477092



Semiclassical wave packet calculations on ion–molecule reactions: Studies on $B^+(^3P_u) + H_2$ reaction

Amrendra Vijay and G. D. Billing

Kemisk Laboratorium III, H. C. Ørsted Institute, University of Copenhagen, DK-2100 Copenhagen Ø, Denmark

(Received 27 February 1997; accepted 19 May 1997)

We present the investigations of nonadiabatic scattering processes (reactive as well charge-transfer) occurring in $B^+ + H_2$ reaction in the gas phase on the triplet electronic surfaces utilizing a mixed quantum-classical approach to scattering of three particle systems in hyperspherical coordinates. The time-dependent Schrödinger equation is solved in diabatic representation using wave packet propagation method on a grid in two quantum dimensions. The potential-energy surfaces have been obtained using the valence-bond diatomics-in-molecule approach. © 1997 American Institute of Physics. [S0021-9606(97)00832-5]

I. INTRODUCTION

Nonadiabatic scattering processes occur frequently between molecular species, with the typical example being the low-energy charge-transfer process between ions and molecules. These processes are of much interest because they are encountered in many systems of major importance for example, plasmas, combustion, fusion, atmospheric chemistry, etc. Complete understanding of these complicated systems requires a detailed information on the scattering processes in the elementary systems at the microscopic level, e.g., ranging from state-selected integral total cross section, state-to-state integral cross section to state-to-state differential cross sections. In this context we have recently in a series of papers formulated the nonadiabatic scattering problem for a general triatomic system in diabatic representation within the hyperspherical coordinate framework.^{1–11} As a general scheme we have discussed the full quantum mechanical problem and it is also possible to obtain (within various limits) a hierarchy of semiclassical schemes suitable for a large spectrum of interesting problems. Within the semiclassical framework we treat part of the system by classical means, wherein classical degrees of freedom are governed by an effective potential, which is an average over the remaining quantum degrees of freedom in the system. This gives rise to a class of hybrid theory in which classical and quantum mechanics are blended in a consistent manner. This approach is sometimes also called the mixed quantum-classical method.¹¹ As the exact quantum mechanical treatment of scattering processes of three particles involving several coupled electronic surfaces is still rather elaborate and time consuming, the mixed quantum-classical approach offers an enormous possibility for treating such systems. In this paper we report our study on $B^+ + H_2$ reaction using a class of mixed quantum-classical approach on the triplet DIM (diatomics in molecules) potential-energy surfaces. Within the hyperspherical coordinate system of this approach we treat the hyper-radius (ρ) and the overall rotational motion described by three Euler angles (α , β , and γ) and their conjugate momenta by classical means and the hyperangles (θ and ϕ) quantum mechanically. However, the introduction of hy-

perspherical coordinates allow the even-handed treatment of all the rearrangement channels, this essentially transforms the reactive scattering problem into an inelastic one. The resulting equations are then convenient to use as they allow for an asymptotic quantization of the vibrational and rotational degrees of freedom of the diatomic fragments, whereas the rotational projection quantum number is treated classically. Thus the initialization of the wave packet as well as the final projection is carried out using asymptotic states which are eigenfunctions of the asymptotic Hamiltonian. In the quantum treatment of hyperangles the corresponding 2D wave packet is propagated on a rectangular grid by the standard Lanczos scheme. A manifold of nine diabatic potential-energy surfaces for the triplet electronic states has been constructed using the valence bond diatomics-in-molecules (VB-DIM) approach of Faist and Muckerman.^{12,13} Prior to this work the dynamical calculations reported on $B^+(^3P_u) + H_2$ system is the quasiclassical trajectory studies on the ground state LEPS triplet surface fitted to *ab initio* points by Klimo *et al.*¹⁴ On the experimental side product angular and energy distribution of this reaction has been studied by Friedrich and Herman.¹⁵ Emission spectroscopic studies on this reaction has been reported by Ottinger and Reichmuth.¹⁶ The outline of the paper is as follows: Section II presents a brief outline of the theory and in Sec. III we present the derivation of potential-energy matrix. The results are presented and discussed in Sec. IV.

II. THEORY

In this section we present a brief overview of the theory we have employed for solving the scattering problem of $B^+ + H_2$ system. For more complete discussion readers may refer to Refs. 1–11. For a general multi-surface problem the time-dependent Schrödinger equation for nuclear motion in diabatic representation is written as

$$i\hbar \frac{\partial}{\partial t} \{ \Xi_k \} = \hat{T} \{ \Xi_k \} + \mathbf{V} \{ \Xi_k \}, \quad (1)$$

where \hat{T} is the usual nuclear kinetic-energy operator and \mathbf{V} is the diabatic potential-energy matrix. The index k refers to

the manifold of diabatic states and the braces denotes the column vector. In the hyperspherical formulation of the $A + BC$ scattering problem the internal configuration of the system is described by the hyper-radius ρ and the two hyper-angles θ and ϕ . The orientation of the ABC triangle in the space-fixed coordinate is described by the Euler angles α , β , and γ . We choose the external coordinate in such a way that the momenta conjugate to α and β are constants of motion, and hence only γ enters the Hamiltonian. By introducing a classical description of γ , ρ and their conjugate momenta, P_γ and P_ρ , respectively, the semiclassical expression for the kinetic-energy term \hat{T} expressed in these coordinates (which are closely related to those of Johnson^{17,18}) takes the form

$$\hat{T} = \frac{P_\rho^2}{2\mu} + \hat{H}_0(\rho, \theta, \phi) + \hat{H}_1(\rho, \theta, \phi, t; J) + \Delta V(\rho, \theta), \quad (2)$$

where

$$\hat{H}_0 = -\frac{2\hbar^2}{\mu\rho^2} \left[\frac{\partial^2}{\partial\theta^2} + \frac{1}{\sin^2\theta} \frac{\partial^2}{\partial\phi^2} \right], \quad (3)$$

$$\hat{H}_1 = \frac{P_\gamma[P_\gamma - 4 \cos\theta \hat{P}_\phi]}{2\mu\rho^2 \sin^2\theta} + \frac{P_J^2 - P_\gamma^2}{\mu\rho^2 \cos^2\theta} \times (1 + \sin\theta \cos 2\gamma), \quad (4)$$

$$\hat{P}_\phi = -i\hbar \frac{\partial}{\partial\phi}, \quad (5)$$

$$\Delta V = -\frac{\hbar^2}{2\mu\rho^2} \left[\frac{1}{4} + \frac{4}{\sin^2 2\theta} \right], \quad (6)$$

and $\mu = \sqrt{m_A m_B m_C} / (m_A + m_B + m_C)$ is the reduced mass for three particles. The potential ΔV is called the extra potential which arises from the kinetic-energy term when transforming from the Cartesian (or Jacobi) to the hyperspherical coordinates, and thus it is independent of electronic states. In the diabatic representation ΔV thus forms a diagonal (constant) matrix which is added to the real potential term in the present discussion. The time-dependent Schrödinger equation [Eq. (1)] is solved by using a 2D-grid representation of the wave function and the Lanczos time propagator. The time dependence arising out of the classical variables is obtained by solving the equations of motion:

$$\dot{\gamma} = \frac{\partial H_{\text{eff}}(P_\gamma, \gamma, P_\rho, \rho, t)}{\partial P_\gamma}, \quad (7)$$

$$\dot{P}_\gamma = -\frac{\partial H_{\text{eff}}(P_\gamma, \gamma, P_\rho, \rho, t)}{\partial \gamma}, \quad (8)$$

$$\dot{\rho} = \frac{P_\rho}{\mu}, \quad (9)$$

$$\dot{P}_\rho = -\frac{\partial H_{\text{eff}}(P_\gamma, \gamma, P_\rho, \rho, t)}{\partial \rho}. \quad (10)$$

Here dot denotes the time derivative. The effective Hamiltonian H_{eff} is obtained as the expectation value of the Hamiltonian, that is

$$H_{\text{eff}} = \frac{P_\rho^2}{2\mu} + \sum_k \langle \Xi_k | \hat{H}_0 | \Xi_k \rangle + \sum_k \langle \Xi_k | \hat{H}_1 | \Xi_k \rangle + V_{\text{eff}}(\rho), \quad (11)$$

where brackets denote average values over θ and ϕ and the effective potential $V_{\text{eff}}(\rho)$ is given as

$$V_{\text{eff}}(\rho) = \langle \{ \Xi_k \}^T [\mathbf{V} + \mathbf{I} \Delta V] \{ \Xi_k \} \rangle. \quad (12)$$

The initial values of the classical variables are

$$\begin{aligned} \rho & \text{ large, } P_\rho = -\sqrt{2\mu(E - \langle (\hat{H}_0 + \mathbf{V} + \mathbf{I} \Delta V) \rangle - \langle \hat{H}_1 \rangle)}, \\ \gamma & \text{ between } 0 \text{ and } 2\pi, P_\gamma \text{ between } -P_J \text{ to } +P_J, \end{aligned} \quad (13)$$

where the brackets indicate that the expectation value is being taken. Since for a given total energy and angular momentum the values of γ and $P_\gamma = J_z$ are not specified, the state to state probabilities are averaged over a number of trajectories (typically several hundred) with appropriately selected initial values of γ and P_γ . To this end we have implemented a Monte Carlo sampling scheme for the selection of γ and P_γ within the largest specified value of $J_z = J_{\text{max}}$ (*vide infra*). Such a procedure represents an average over the initial and a sum over the final projection quantum numbers. For each selected values of γ and P_γ a trajectory is propagated in ρ inwards, it reaches a turning point and moves out again. It is then terminated at a large value of ρ (6 Å or more). The distribution of γ is not uniform in the above range [cf. Eq. (13)] and thus the values of P_γ and γ have to be compatible with the constraint that $|\kappa|$ (*vide infra*) be smaller than j .

A. Initialization

The initial wave function is taken as a product of a Morse vibrational and an Arthurs–Dalgarno state \mathcal{Y}_{jl}^{jm} for the internal motion of the diatomics. The initial wave function determines the ‘ K -component’ of the wave packet expressed in terms of the hyperspherical coordinates

$$\Xi_J = \sum_{-J}^J \Xi_K^J(\theta, \phi; \rho) D_{MK}^J(\alpha, \beta, \gamma), \quad (14)$$

where D_{MK}^J are the rotation matrix elements. If the vibrational and rotational degrees of freedom are treated as separable, we can write the wave function of the diatomic molecule BC as

$$s_{vjm}(r, \eta, \xi) = g_v(r) Y_{jm}(\eta, \xi), \quad (15)$$

where g is the vibrational wave function and Y is a spherical harmonic function. In the present semiclassical approximation the Euler angles are treated classically. As a result, the angle ξ (which is related to the Euler angles), that is, the rotational projection states are also treated classically and hence the eigenstates of BC molecule may be labeled by v and j only. We thus write the wave function of the diatomic molecule BC as

$$s_{vj}(r, \eta; \kappa) = \frac{1}{\sqrt{x}} g_{vj}(x) P_j^\kappa(\cos \eta) \sqrt{\sin \eta}. \quad (16)$$

The significance of index κ , quantity x and other factors will be explained later. Here P_j is the normalized Legendre function. Thus the total wave function put on the two-dimensional grid is given as

$$\Xi(\theta, \phi; \rho) = \rho s_{vj}(r, \eta; \kappa). \quad (17)$$

Now we discuss the asymptotic mapping of the Hamiltonian leading to different arrangement channels. The asymptotic mapping can be obtained by introducing two variables x and η such that

$$\theta = \frac{\pi}{2} - \frac{x}{\rho} \sin \eta, \quad (18)$$

$$\phi = \phi_0 + \frac{x}{\rho} \cos \eta, \quad (19)$$

where ϕ_0 is a channel dependent angle and the variable x is related to the diatomic internuclear distance r

$$r = \frac{d_i x}{2}, \quad (20)$$

where $d_i^2 = (m_i/\mu)(1 - m_i/M)$ and the index i refers to the channel. Here $M = m_A + m_B + m_C$ is the total mass of the system. On inserting the above representation of θ and ϕ in Eqs. (2)–(6) the total nuclear Hamiltonian, \hat{H}_{nu} [cf. Eq. (1)] transforms to

$$\begin{aligned} \hat{H}_{nu} \rightarrow & \frac{P_\rho^2}{2\mu} - \frac{2\hbar^2}{\mu} \left(\frac{\partial^2}{\partial x^2} + \frac{1}{x} \frac{\partial}{\partial x} - \frac{1}{4x^2} \right) + \mathbf{V}(x) \\ & - \frac{2\hbar^2}{\mu x^2} \left(\frac{\partial^2}{\partial \eta^2} + \frac{1}{4 \sin^2 \eta} + \frac{1}{4} \right) \\ & + \frac{P_J^2 - P_\gamma^2}{\mu x^2 \sin^2 \eta} [1 + \cos(2\gamma)]. \end{aligned} \quad (21)$$

Now it is fairly straightforward to verify that the diatomic wave function ζ_{vj} [Eq. (16)] is the eigen function of the above asymptotic Hamiltonian. We therefore come to the conclusion that the nuclear wave function Ξ can be labeled asymptotically by the vibrational quantum number v of a one dimensional oscillator and by a rotational quantum number j . Hence a quantum mechanical treatment of the hyperspherical variables θ and ϕ asymptotically corresponds to a quantum treatment of the vibrational and rotational motion, whereas the rotational projection is treated classically. It can be shown⁴ that η in the definition of wave function [Eq. (16)] is the angle between the distance from the atom A to the center of mass of the diatomic molecule BC and the r axis and is given as

$$\eta = -\arccos\left(\frac{\sin \theta \sin \phi}{\sqrt{1 - \sin^2 \theta \cos \phi}}\right). \quad (22)$$

Note that the inclusion of factor ρ and $\sqrt{\sin(\eta)}$ in the definition of wave function [Eqs. (16) and (17)] ensures the correct volume element in terms of the hyperspherical variables. The

index κ in the definition of the wave function [Eq. (16)] is a continuous quantity obtained from the solution to the differential Eq. (21) and is given as

$$\kappa = \frac{\cos \gamma}{\hbar} \sqrt{P_J^2 - P_\gamma^2}. \quad (23)$$

In the actual implementation we select κ randomly between $-(j + \frac{1}{2})$ and $+(j + \frac{1}{2})$ and P_γ between $-P_J$ and $+P_J$ and obtain

$$\gamma = \arccos(\hbar \kappa / \sqrt{P_J^2 - P_\gamma^2}). \quad (24)$$

The weight of a given K state, where $P_\gamma = \hbar K$ is given as

$$\begin{aligned} w_K &= \frac{1}{\pi} \int_{\gamma_-}^{\gamma_+} d\gamma \\ &= \frac{1}{\pi} \arcsin\left(\frac{\kappa}{\sqrt{(J + \frac{1}{2})^2 - K^2}}\right) \Bigg|_{-(j + \frac{1}{2})}^{+(j + \frac{1}{2})}, \end{aligned} \quad (25)$$

where γ_- and γ_+ are the extremes corresponding to the two limiting values of κ , i.e., $\pm(j + \frac{1}{2})$. Thus we have

$$w_K = \frac{2}{\pi} \arcsin\left(\frac{j + \frac{1}{2}}{\sqrt{(J + \frac{1}{2})^2 - K^2}}\right). \quad (26)$$

Now in the limit of large values of j we can also approximate the Legendre function as follows:

$$P_j^\kappa = \sqrt{\frac{2}{\pi \sin \eta}} \cos\left[\left(j + \frac{1}{2}\right)\eta - \frac{\pi}{4} + \frac{\kappa \pi}{2}\right]. \quad (27)$$

In the present study we take g [cf. Eq. (16)] as Morse oscillator function. Finally we note that the asymptotic wave function Ξ will also be characterized by the arrangement channel c (1 for $B+H_2$, 2 for H_b+BH_a , and 3 for H_a+H_bB). We start the calculation after initializing the wave packet at large ρ ($\sim 6 \text{ \AA}$) on the ground $^3A'$ potential surface. We note that the lowest two DIM surfaces are degenerate in the entrance channel ($B^+ + H_2$), and hence the initialization consists of the linear combination of the two surfaces. Thus the initial wave function is put on the equidistant grid (of size 128×32 for $\phi \times \theta$) using the relation (16). The classical equations of motion for ρ , P_ρ , γ , and P_γ are solved simultaneously with the wave packet propagation.

B. Asymptotic projection

The outgoing wave packet carries the scattering information for all arrangement channels. The analysis is performed at large value of ρ when the coupling is assumed to be negligible. In order to obtain the scattering amplitudes for specific vibrational–rotational transitions we have to evaluate the following integral:

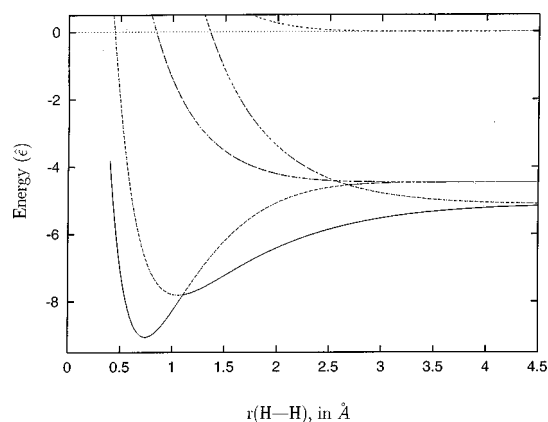


FIG. 1. DIM $^3A'$ potential-energy surface in the entrance channel ($B^+ + H_2$).

$$a_{vj} = \int d\theta \int d\phi \Xi^*(\theta, \phi; \rho) \times \frac{\rho}{\sqrt{x}} \sqrt{\sin \eta} g_v(x) P_j^{\kappa}(\cos \eta), \quad (28)$$

where x and η are functions of θ and ϕ . Due to coarse grid used in the present study it was not possible to resolve the rotational state distribution, and therefore, we have obtained the rotationally averaged vibrational cross sections by a recently proposed projection scheme.¹ In this scheme we project the scattered wave function onto the rotationally summed product vibrational states and compute the transition probabilities¹ as

$$P_v = 2\rho^2 \int d\theta \int d\phi \int d\theta' \int d\phi' \Xi^*(\theta, \phi; \rho) \times \Xi(\theta', \phi'; \rho) g_v(x') g_v(x) \frac{\delta(\eta - \eta')}{\sqrt{xx'}}. \quad (29)$$

The interesting feature of this projection scheme is the presence of delta function (which appears as a result of taking the limit large j_{\max} tending to ∞) which reduces the above four-dimensional integral to a three-dimensional one and since the main contribution comes from $\theta \sim \theta'$ and $\phi \sim \phi'$, the above integral becomes actually a two-dimensional one. As we show in Fig. 1 two potential-energy surfaces asymptotically cross each other at some point, and thus while computing the reaction probabilities one has to account for this. To this end we have followed the scheme as discussed in Ref. 4. In brief, the scattered wave packet is first transformed to the adiabatic representation by diagonalizing the potential-energy matrix at each grid point and using the corresponding eigenvectors. And while computing the total probability on an individual surface, we reverse the contribution at the crossing point as it is easy to identify the surface characteristics for different species. Finally the scattered wave packet on different surfaces are projected onto the asymptotic states of the corresponding product species.

Total reaction probabilities are obtained by integrating the square of the scattered wave function over regions of the

grid corresponding to the different channels—this method is also called “grid summation.” For this purpose we partition the grid in ϕ space into three parts corresponding to three different arrangement channel. We have obtained the correct point of partition in the ϕ space by examining the potential-energy surface in the region. In the present case, two arrangement channels are equivalent for symmetry reason and thus the final cross sections have to be added. The so called grid summation method is particularly useful because the problem of resolving highly excited states on a coarse grained grid is avoided, of course at the cost of losing information on the product internal energy distribution.

III. POTENTIAL-ENERGY SURFACES

We have constructed the diabatic potential-energy surfaces for the triplet states of $B^+ + H_2$ system using the VB-DIM scheme of Faist and Muckerman.^{12,13} As we have explained in the Appendix the final equation to obtain the potential-energy matrix for a three particle system reads as follows:

$$H_{\text{DIM}} = \sum_p \sum_{q>p} \tilde{H}^{pq} - (N-2) \sum_p \tilde{H}^p, \quad (30)$$

where

$$\begin{aligned} \tilde{H}^{pq} &= F_{(pq)}^\dagger Q_{pq} H_{\Psi pq} Q_{pq}^\dagger F_{(pq)}, \\ \tilde{H}^p &= F_{(p)}^\dagger H_{\Psi p} F_{(p)}. \end{aligned} \quad (31)$$

Here the indices p and q refer to the atoms in the molecule. We use the DIM Eq. (31) in its semiempirical framework wherein we substitute $H_{\Psi p}$ in Eq. (24) by the information externally obtained from other sources. The required information is the atomic energies and various diatomic potential-energy curves. In the following we briefly describe how to obtain the fragment matrices \tilde{H}^p with a few illustrative tables. The possible atomic fragments (p) in the present molecule are H^+ , B^+ , B , H_a , and H_b where we have labeled the two hydrogen atoms by a and b , respectively. For diatomic fragments (pq) we have the possibilities: H_2 , BH_a , BH_b , BH_a^+ , BH_b^+ , and H_2^+ . The idea behind the DIM method is to construct the polyatomic wave function using the valence bond (VB) wave functions in such a manner that the polyatomic wave function correlates with the VB functions of the fragments. The wave functions are properly antisymmetrized, that is they are built of Slater determinants.

In order to construct the DIM potential-energy matrix we have employed the following three basic structures:

- (1) $B^+(^1S) + 2H(1s)$,
- (2) $B^+(^3P) + 2H(1s)$,
- (3) $B(^2P) + H(1s) + H^+$,

which gives rise to a manifold of nine diabatic $^3A'$ states. In the construction of valence bond polyatomic basis functions (pbf) we align the p_z spin-orbital of the B atom to be directed towards H_a and the p_x spin-orbital of the B atom to be contained in the plane of the molecule (C_s point group).

TABLE I. Polyatomic basis functions^a of (BH₂)⁺.

	Basis set	Symmetry description
1.	$\frac{1}{\sqrt{2}} \{ s\bar{s}\bar{a}\bar{b}\rangle + s\bar{s}\bar{a}\bar{b}\rangle\}$	$B^+(^1S_g) + H_2(^3\Sigma_u^+)$
2.	$\frac{1}{\sqrt{2}} \{ s\bar{s}\bar{z}\bar{a}\bar{b}\rangle - s\bar{s}\bar{z}\bar{a}\bar{b}\rangle\}$	$B^+_z(^3P_u) + H_2(^3\Sigma_u^+)$
3.	$\frac{1}{\sqrt{2}} \{ s\bar{s}\bar{z}\bar{a}\bar{b}\rangle + s\bar{s}\bar{z}\bar{a}\bar{b}\rangle - s\bar{s}\bar{z}\bar{a}\bar{b}\rangle - s\bar{s}\bar{z}\bar{a}\bar{b}\rangle\}$	$B^+_z(^3P_u) + H_2(^1\Sigma_g^+)$
4.	$\frac{1}{\sqrt{2}} \{ s\bar{s}\bar{x}\bar{a}\bar{b}\rangle - s\bar{s}\bar{x}\bar{a}\bar{b}\rangle\}$	$B^+_x(^3P_u) + H_2(^3\Sigma_u^+)$
5.	$\frac{1}{\sqrt{2}} \{ s\bar{s}\bar{x}\bar{a}\bar{b}\rangle + s\bar{s}\bar{x}\bar{a}\bar{b}\rangle - s\bar{s}\bar{x}\bar{a}\bar{b}\rangle - s\bar{s}\bar{x}\bar{a}\bar{b}\rangle\}$	$B^+_x(^3P_u) + H_2(^1\Sigma_g^+)$
6.	$\frac{1}{\sqrt{2}} \{ s\bar{s}\bar{s}\bar{z}\bar{a}\rangle + s\bar{s}\bar{s}\bar{z}\bar{a}\rangle\}$	$B_z(^2P_u) + H_2(^2S_g)$
7.	$\frac{1}{\sqrt{2}} \{ s\bar{s}\bar{s}\bar{x}\bar{a}\rangle + s\bar{s}\bar{s}\bar{x}\bar{a}\rangle\}$	$B_x(^2P_u) + H_2(^2S_g)$
8.	$\frac{1}{\sqrt{2}} \{ s\bar{s}\bar{s}\bar{z}\bar{b}\rangle + s\bar{s}\bar{s}\bar{z}\bar{b}\rangle\}$	$B_z(^2P_u) + H_2(^2S_g)$
9.	$\frac{1}{\sqrt{2}} \{ s\bar{s}\bar{s}\bar{x}\bar{b}\rangle + s\bar{s}\bar{s}\bar{x}\bar{b}\rangle\}$	$B_x(^2P_u) + H_2(^2S_g)$

^aSee the text for the meaning of the symbols.

Further we assume that the use of one electron spin-orbitals through only the valence shell is appropriate for the purpose. Designating the 1s orbital of the hydrogen atoms by the letter *a* and *b*, and the 2s, 2*p_x*, and 2*p_z* atomic orbitals of *B* atom by the letter *s*, *x*, and *z*, respectively, Table I shows the nine possible primitive *pbf* for the (BH₂)⁺ system. In the sequel we present the basis sets for the different fragments in Tables II–V. In the following we illustrate the construction of the transformation matrix $F_{(\nu)}$ for one fragment BH_{*a*}. For other fragments these matrices are constructed in a similar fashion and thus they are not reproduced here for brevity.

A. Fragment matrices

The construction of the matrix $F_{(\nu)}$ [cf. Eq. (31)] follows Ref. 13. We suppress the details and give only the final expression here

$$F_{(\nu)} = C_{\nu}^{-1} G_{(\nu)}. \quad (32)$$

If we compose a row vector $f_{(\nu)}$ of the ν -fragment Slater determinant then the transformation matrix $G_{(\nu)}$ is composed of not- ν slater determinant with a phase factor $(-1)^l$, where *l* is the number of permutations required to reorder the elec-

TABLE II. Basis set^a for hydrogen atom.

	Basis set	Symmetry species
1.	<i>a</i> (<i>b</i>)	2S_g
2.	\bar{a} (\bar{b})	2S_g
3.	1	1S_g

^aSee the text for the meaning of the symbols.

TABLE III. Basis set^a for H₂ fragment.

	Basis set	Symmetry species
1.	$\frac{1}{\sqrt{2}} \{ a\bar{b}\rangle - \bar{a}b\rangle\}$	$^1\Sigma_g^+$
2.	$\frac{1}{\sqrt{2}} \{ a\bar{b}\rangle + \bar{a}b\rangle\}$	$^3\Sigma_u^+$
3.	<i>ab</i>	$^3\Sigma_u^+$
4.	$\bar{a}\bar{b}$	$^3\Sigma_u^+$
5.	$\frac{1}{\sqrt{2}} \{a+b\}$	2S_g
6.	$\frac{1}{\sqrt{2}} \{\bar{a}+\bar{b}\}$	2S_g
7.	$\frac{1}{\sqrt{2}} \{a-b\}$	2S_g
8.	$\frac{1}{\sqrt{2}} \{\bar{a}-\bar{b}\}$	2S_g

^aSee the text for the meaning of the symbols.

trons and the matrix C_{ν} connects the row vector $f_{(\nu)}$ to the basis set of ν fragment via a square transformation. We thus have

$$\Psi_{(BH_a)} = f_{(BH_a)} C_{BH_a}, \quad (33)$$

$$\Psi_{(pbf)} = f_{(BH_a)} G_{(BH_a)}.$$

We note that the matrix C_{ν} is unitary under the ZAO (zero overlap of atomic orbitals) approximation and hence $C_{\nu}^{-1} = C_{\nu}^{\dagger}$. Referring to Table V we write the row vector f_{BH_a} as follows:

$$f_{(BH_a)} = \{ |s\bar{s}\bar{\sigma}\bar{a}\rangle, |s\bar{s}\bar{\sigma}a\rangle, |s\bar{s}\bar{\pi}\bar{a}\rangle, |s\bar{s}\bar{\pi}a\rangle, |s\bar{s}\bar{a}\rangle, |s\bar{s}\bar{\sigma}\rangle, |s\bar{s}\bar{\sigma}\bar{a}\rangle, |s\bar{s}\bar{\sigma}a\rangle, |s\bar{s}\bar{\pi}\bar{a}\rangle, |s\bar{s}\bar{\pi}a\rangle, |s\bar{s}\bar{a}\rangle, |s\bar{s}\bar{\sigma}\rangle, |s\bar{s}\bar{\sigma}\bar{a}\rangle, |s\bar{s}\bar{\sigma}a\rangle, |s\bar{s}\bar{\pi}\bar{a}\rangle, |s\bar{s}\bar{\pi}a\rangle, |s\bar{s}\bar{a}\rangle, |s\bar{s}\bar{\sigma}\rangle, |s\bar{s}\bar{\sigma}\bar{a}\rangle, |s\bar{s}\bar{\sigma}a\rangle, |s\bar{s}\bar{\pi}\bar{a}\rangle, |s\bar{s}\bar{\pi}a\rangle \}. \quad (34)$$

TABLE IV. Basis set^a for boron atom.

	Basis set	Symmetry species
1.	<i>s</i> $\bar{s}\bar{z}$	$B(^2P_u)$
2.	<i>s</i> $\bar{s}\bar{x}$	$B(^2P_u)$
3.	<i>s</i> $\bar{s}\bar{z}$	$B(^2P_u)$
4.	<i>s</i> $\bar{s}\bar{x}$	$B(^2P_u)$
5.	<i>s</i> \bar{s}	$B^+(^1S_g)$
6.	$\frac{1}{\sqrt{2}} \{ s\bar{z}\rangle + \bar{s}\bar{z}\rangle\}$	$B^+(^3P_u)$
7.	<i>sz</i>	$B^+(^3P_u)$
8.	$\bar{s}\bar{z}$	$B^+(^3P_u)$
9.	$\frac{1}{\sqrt{2}} \{ s\bar{x}\rangle + \bar{s}\bar{x}\rangle\}$	$B^+(^3P_u)$
10.	<i>s</i> \bar{x}	$B^+(^3P_u)$
11.	$\bar{s}\bar{x}$	$B^+(^3P_u)$

^aSee the text for the meaning of the symbols.

TABLE V. Basis set^a for BH fragment.^b

	Basis set	Symmetry species
1.	$\frac{1}{\sqrt{2}} \{ s\bar{s}\sigma\bar{a}\rangle - s\bar{s}\sigma a\rangle\}$	BH($^1\Sigma_0$)
2.	$\frac{1}{\sqrt{2}} \{ s\bar{s}\pi\bar{a}\rangle - s\bar{s}\pi a\rangle\}$	BH($^1\Pi_0$)
3.	$\frac{1}{\sqrt{2}} \{ s\bar{s}\sigma\bar{a}\rangle + s\bar{s}\sigma a\rangle\}$	BH($^3\Sigma_0$)
4.	$\frac{1}{\sqrt{2}} \{ s\bar{s}\pi\bar{a}\rangle + s\bar{s}\pi a\rangle\}$	BH($^3\Pi_0$)
5.	$ s\bar{s}a\rangle$	BH ⁺ ($X^2\Sigma_{1/2}^+$)
6.	$ s\bar{s}\sigma\rangle$	BH ⁺ ($3^2\Sigma_{1/2}^+$)
7.	$\frac{1}{\sqrt{6}} \{2 s\sigma\bar{a}\rangle - s\bar{\sigma}a\rangle - \bar{s}\sigma a\rangle\}$	BH ⁺ ($B'^2\Sigma_{1/2}^+$)
8.	$ s\bar{s}\pi\rangle$	BH ⁺ ($2^2\Pi_{1/2}$)
9.	$\frac{1}{\sqrt{6}} \{2 s\pi\bar{a}\rangle - s\bar{\pi}a\rangle - \bar{s}\pi a\rangle\}$	BH ⁺ ($A^2\Pi_{1/2}$)
10.	$ s\bar{s}a\rangle$	BH ⁺ ($^2\Sigma_{-1/2}$)
11.	$ s\bar{s}\sigma\rangle$	BH ⁺ ($^2\Sigma_{-1/2}$)
12.	$\frac{1}{\sqrt{6}} \{2 \bar{s}\sigma a\rangle - s\sigma\bar{a}\rangle - \bar{s}\sigma\bar{a}\rangle\}$	BH ⁺ ($^2\Sigma_{-1/2}$)
13.	$ s\bar{s}\pi\rangle$	BH ⁺ ($^2\Pi_{-1/2}$)
14.	$\frac{1}{\sqrt{6}} \{2 \bar{s}\pi a\rangle - s\pi\bar{a}\rangle - \bar{s}\pi\bar{a}\rangle\}$	BH ⁺ ($^2\Pi_{-1/2}$)
15.	$\frac{1}{\sqrt{3}} \{ s\sigma\bar{a}\rangle + s\bar{\sigma}a\rangle + \bar{s}\sigma a\rangle\}$	BH ⁺ ($^4\Sigma_{3/2}^+$)
16.	$\frac{1}{\sqrt{3}} \{ s\pi\bar{a}\rangle + s\bar{\pi}a\rangle + \bar{s}\pi a\rangle\}$	BH ⁺ ($^4\Pi_{3/2}$)
17.	$\frac{1}{\sqrt{3}} \{ \bar{s}\sigma a\rangle + s\sigma\bar{a}\rangle + \bar{s}\sigma\bar{a}\rangle\}$	BH ⁺ ($^4\Sigma_{-3/2}$)
18.	$\frac{1}{\sqrt{3}} \{ \bar{s}\pi a\rangle + s\pi\bar{a}\rangle + \bar{s}\pi\bar{a}\rangle\}$	BH ⁺ ($^4\Pi_{-3/2}$)

^aSee the text of the meaning for the symbols.

^bHere σ and π refer to the p_z and p_x orbitals, respectively, of the B atom.

By using Eq. (33) and (34) and referring to Tables I and V we obtain the matrices C_{BH_a} and G_{BH_a} for the BH_a fragment and they are given in Tables VI and VII, and thus we evaluate the matrix F_{BH_a} according to Eq. (32). For the other fragment BH_b we need to account for the directional nature of the p orbitals of B atom as discussed in the Appendix. The transformation matrix Q needed for this purpose is easily obtained by aligning the H_b atom such that the σ orbital is along the BH_b bond. This amounts to the rotation through the angle φ (which is the angle between BH_a and BH_b bonds in the molecule) as follows:

$$[\sigma_b, \pi_b] = [2p_z, 2p_x] \begin{bmatrix} \cos \varphi & -\sin \varphi \\ \sin \varphi & \cos \varphi \end{bmatrix}. \quad (35)$$

Thus the complete rotation matrix which is block diagonal and square (22×22 in the present case) can easily be constructed by referring to Table V and we do not reproduce it

here. Before we finally construct the fragment matrices let us briefly discuss the fragment Hamiltonian ($H_{\Psi\nu}$) in Eq. (31).

If the basis set of a fragment is composed of functions with the different spin and spatial symmetry then the corresponding Hamiltonian matrix is diagonal, and this is the case for all the atomic fragments (B and H) and the diatomic fragment H_2 . For these fragments we substitute the Hamiltonian ($H_{\Psi\nu}$) by the appropriate atomic state energies and the diatomic potential curves. The experimental values for the atomic energies were obtained from the standard atomic energy tables available in the literature.¹⁹ Other relevant data for the present purpose were obtained from Ref. 20. The zero of energy for $(BH_2)^+$ was chosen to be the energy of isolated $B^+(^1S_g)$ and two hydrogen atoms and the energies of the other atomic states are measured with respect to these two. However the fragment matrices corresponding to the diatomics BH require much more work to construct. We notice from Table V that the basis functions 5–7 ($^2\Sigma$), 8 and 9 ($^2\Pi$), 10–12 ($^2\Sigma$) and 13 and 14 ($^2\Pi$) form subgroups with same spin symmetry, and hence the Hamiltonian matrix would contain the off-diagonal terms within these subgroups and the structure of rest of the matrix would be diagonal. The resulting Hamiltonian matrix would thus be block diagonal. We take the adiabatic potential-energy surfaces for the states of a BH fragment which are not coupled. In order to mix the $^2\Sigma$ and $^2\Pi$ states of BH^+ separately we carry out adiabatic–diabatic transformation within these subgroups.²¹ For the $^2\Pi$ states which form a 2×2 sub-matrix let us denote the adiabatic energies as Λ_1 and Λ_2 . The mixing of these two states is carried out as follows:

$$\begin{bmatrix} \Pi_{11} & \Pi_{12} \\ \Pi_{12} & \Pi_{11} \end{bmatrix} = \begin{bmatrix} \cos \vartheta & -\sin \vartheta \\ \sin \vartheta & \cos \vartheta \end{bmatrix} \begin{bmatrix} \Lambda_2 & 0 \\ 0 & \Lambda_1 \end{bmatrix} \times \begin{bmatrix} \cos \vartheta & \sin \vartheta \\ -\sin \vartheta & \cos \vartheta \end{bmatrix}, \quad (36)$$

where ϑ is the mixing angle which is generally a complicated function of bond distance. The $^2\Sigma$ subgroup of BH fragment involve three electronic states, and thus three different mixing angles are required to carry out the transformation. The data for mixing angles as a function of bond distance we have taken from Ref. 20. We are now ready to construct all the fragment matrices. We present the final expression for the DIM matrix for $(BH_2)^+$ in Table VIII. This would be useful for the future work if one needs to incorporate an improved fragment data set.

B. Features of PES

For the analysis purpose we can obtain the adiabatic potential-energy surfaces by diagonalizing the DIM matrix (Table VIII). For this system we find that in the entrance channel four lowest potential surfaces form two degenerate sets corresponding to $B^+(^3P) + H_2(^1\Sigma_g^+)$, and $B(^2P) + H_2(^2\Sigma_g^+)$ asymptotes and the remaining five upper surfaces are repulsive in nature (see Fig. 1). In the reactive channel potential surfaces of interest are those corresponding to the products $BH^+(X^2\Sigma^+)$, $BH^+(B^2\Sigma^+)$, and $BH(X^1\Sigma^+)$. In the discussion of reaction dynamics it is

TABLE VI. The matrix C_v for the BH_a fragment.

$\frac{1}{\sqrt{2}}$	0	$\frac{1}{\sqrt{2}}$	0	0	0	0	0	0	0	0	0	0	0	0	0	0	0
$-\frac{1}{\sqrt{2}}$	0	$\frac{1}{\sqrt{2}}$	0	0	0	0	0	0	0	0	0	0	0	0	0	0	0
0	$\frac{1}{\sqrt{2}}$	0	$\frac{1}{\sqrt{2}}$	0	0	0	0	0	0	0	0	0	0	0	0	0	0
0	$-\frac{1}{\sqrt{2}}$	0	$\frac{1}{\sqrt{2}}$	0	0	0	0	0	0	0	0	0	0	0	0	0	0
0	0	0	0	1	0	0	0	0	0	0	0	0	0	0	0	0	0
0	0	0	0	0	1	0	0	0	0	0	0	0	0	0	0	0	0
0	0	0	0	0	0	$\frac{2}{\sqrt{6}}$	0	0	0	0	0	0	0	$\frac{1}{\sqrt{3}}$	0	0	0
0	0	0	0	0	0	$-\frac{1}{\sqrt{6}}$	0	0	0	0	0	0	0	$\frac{1}{\sqrt{3}}$	0	0	0
0	0	0	0	0	0	$-\frac{1}{\sqrt{6}}$	0	0	0	0	0	0	0	$\frac{1}{\sqrt{3}}$	0	0	0
0	0	0	0	0	0	0	1	0	0	0	0	0	0	0	0	0	0
0	0	0	0	0	0	0	0	$\frac{2}{\sqrt{6}}$	0	0	0	0	0	0	$\frac{1}{\sqrt{3}}$	0	0
0	0	0	0	0	0	0	0	$-\frac{1}{\sqrt{6}}$	0	0	0	0	0	0	$\frac{1}{\sqrt{3}}$	0	0
0	0	0	0	0	0	0	0	$-\frac{1}{\sqrt{6}}$	0	0	0	0	0	0	$\frac{1}{\sqrt{3}}$	0	0
0	0	0	0	0	0	0	0	0	1	0	0	0	0	0	0	0	0
0	0	0	0	0	0	0	0	0	0	1	0	0	0	0	0	0	0
0	0	0	0	0	0	0	0	0	0	0	$\frac{2}{\sqrt{6}}$	0	0	0	0	$\frac{1}{\sqrt{3}}$	0
0	0	0	0	0	0	0	0	0	0	0	$-\frac{1}{\sqrt{6}}$	0	0	0	0	$\frac{1}{\sqrt{3}}$	0
0	0	0	0	0	0	0	0	0	0	0	$-\frac{1}{\sqrt{6}}$	0	0	0	0	$\frac{1}{\sqrt{3}}$	0
0	0	0	0	0	0	0	0	0	1	0	0	1	0	0	0	0	0
0	0	0	0	0	0	0	0	0	0	0	0	0	$\frac{2}{\sqrt{6}}$	0	0	0	$\frac{1}{\sqrt{3}}$
0	0	0	0	0	0	0	0	0	0	0	0	0	$-\frac{1}{\sqrt{6}}$	0	0	0	$\frac{1}{\sqrt{3}}$
0	0	0	0	0	0	0	0	0	0	0	0	0	$-\frac{1}{\sqrt{6}}$	0	0	0	$\frac{1}{\sqrt{3}}$

useful to construct a correlation diagram showing the correlation between the reactant and product states. Here we discuss the correlation pertinent to the present study only. On the ${}^3A'$ potential surfaces the reactant $B^+({}^3P) + H_2(1\Sigma_g^+)$ correlate with the ground-state product $BH^+(X\ 2\Sigma^+) + H(2S_g)$. This qualitatively means that if the scattering takes place only on the lowest adiabatic surface then $BH^+(X\ 2\Sigma^+)$ would be the only outcome. However, if the scattering event is nonadiabatic in nature there would be the possibility of charge transfer giving rise to the $B(2P) + H_2(2\Sigma_g^+)$ product. Now $B(2P) + H_2(2\Sigma_g^+)$ channel also correlate with the $BH^+(B\ 2\Sigma^+) + H(2S_g)$ asymptote. Hence

if the scattering is nonadiabatic and the charge transfer step is an efficient one, there would be much possibility of the formation of excited-state product $BH^+(B\ 2\Sigma^+)$ in comparison to that of the ground-state product $BH^+(X\ 2\Sigma^+)$. As we shall see later this is the outcome of the present calculations. In Fig. 2 we give the contour plot of the potential-energy surfaces obtained presently in the hyperspherical variables. We show the contour in θ and ϕ space at small ρ ($2\ \text{\AA}$) which approximately corresponds to the classical turning point in the ρ motion for this reaction (Fig. 2). The present reaction is an example of exothermic one without any barrier. In Fig. 3 we plot the potential surfaces for the collinear

TABLE VII. The matrix $G_{(v)}$ for the BH_a fragment.

0	0	0	0	0	$\frac{1}{\sqrt{2}}$	0	0	0
0	0	0	0	0	$\frac{1}{\sqrt{2}}$	0	0	0
0	0	0	0	0	0	$\frac{1}{\sqrt{2}}$	0	0
0	0	0	0	0	0	$\frac{1}{\sqrt{2}}$	0	0
$\frac{\bar{b}}{\sqrt{2}}$	0	0	0	0	0	0	0	0
0	0	0	0	0	0	0	$\frac{\bar{b}}{\sqrt{2}}$	0
0	$-\frac{\bar{b}}{\sqrt{2}}$	0	0	0	0	0	0	0
0	0	$\frac{\bar{b}}{2}$	0	0	0	0	0	0
0	0	$\frac{\bar{b}}{2}$	0	0	0	0	0	0
0	0	0	0	0	0	0	0	$\frac{\bar{b}}{\sqrt{2}}$
0	0	0	$-\frac{\bar{b}}{\sqrt{2}}$	0	0	0	0	0
0	0	0	0	$\frac{\bar{b}}{2}$	0	0	0	0
0	0	0	0	$\frac{\bar{b}}{2}$	0	0	0	0
$\frac{b}{\sqrt{2}}$	0	0	0	0	0	0	0	0
0	0	0	0	0	0	0	$\frac{b}{\sqrt{2}}$	0
0	$\frac{b}{\sqrt{2}}$	0	0	0	0	0	0	0
0	0	$-\frac{b}{2}$	0	0	0	0	0	0
0	0	$-\frac{b}{2}$	0	0	0	0	0	0
0	0	0	0	0	0	0	0	$\frac{b}{\sqrt{2}}$
0	0	0	$\frac{b}{\sqrt{2}}$	0	0	0	0	0
0	0	0	0	$-\frac{b}{2}$	0	0	0	0
0	0	0	0	$-\frac{b}{2}$	0	0	0	0

approach. We note that the third electronic state in Fig. 3, which gives the excited-state product $BH^+(B^2\Sigma^+)$, has a barrier in the exit channel.

IV. RESULTS AND DISCUSSION

We have performed the 2D wave packet calculations from the ground ro-vibrational state of $B^+ + H_2$ on the triplet

surface at a range of energies from $0.5\hat{\epsilon}$ to $7.0\hat{\epsilon}$ ($1\hat{\epsilon} = 100$ KJ/mol). As we discussed earlier for a given total energy the values of γ and P_γ are not specified, we have therefore taken average over a number of trajectories with different initial γ and P_γ in order to obtain the scattering amplitudes. Note that for each trajectory one has to solve the full 2D quantum problem. In order to obtain the converged result with respect to J we have carried out calculations in several batches for a given range $J_{\min} \leq J \leq J_{\max}$ (the range containing typically 50 values) and introduce a random selection of P_γ between $-P_J$ and P_J , and the values of γ are obtained from the random selection of the quantity κ [cf. Eq. (24)]. For each range of J values we average over typically 50–100 trajectories which was sufficient to obtain the convergence within the range. And finally the contribution from different range of J values to the reaction cross sections were added. For a given energy typically $0 \leq J \leq 350$ range contributes to the scattering amplitudes, though for lower energy we obtain the convergence for a smaller range only. The initial condition of the reaction here represents the $B^+(^3P)$ atom colliding with the H_2 molecule in its ground state. The propagation was carried out in the diabatic representation with continuous coupling between different electronic states. The evaluation of the quantum part of the system makes use of standard FFT method on an evenly spaced grid. As the wave packet must be zero for both $\theta=0$ and $\pi/2$ on the grid it is not necessary to determine the time evolution of the wave packets for these values of θ . We note that at these values of theta the extra potential term ΔV is singular and the large values of $V + \Delta V$ makes the numerical calculation somewhat unstable. This deficiency was overcome by limiting the value of the potential to a fixed value in the strongly forbidden classical region where the wave packet never reaches, and hence for the first few values of theta we put the wave packet to zero. The time-dependent Schrödinger equation is solved by the standard short time iterative Lanczos method with a fixed time step 0.005τ ($1\tau = 10$ fs). Typically 10–15 Lanczos iterations were required to obtain a good accuracy in the calculations. Along the ρ coordinate we carry out the classical propagation from large ρ inward and the system reaches the classical turning point (typically at $\rho \sim 2 \text{ \AA}$) and then it comes out. At the end of the collision we have the scattered wave packets on all the electronic surfaces which contain all the information of collision. The scattered wave packets are analyzed as explained earlier. For illustration in Fig. 4 we give the probability amplitude plot of the scattered wave packet at $1\hat{\epsilon}$ energy on different electronic states at the end of collision. We note, for example from Fig. 1, that some of the surfaces are repulsive in nature and therefore we should not expect any probability contribution to these surfaces. In practice, however, there is small contribution of probability to the closed channels (in the present case it is negligible compared to the open channels), and this is due to the semiclassical nature of the method we have utilized presently.

We present the total cross sections vs energy for different products in Table IX. As is clearly seen from the Table

TABLE VIII. The DIM potential-energy matrix^a for (BH₂)⁺.

$H(1,1) = {}^2\Sigma_{11}(\text{BH}_a) + {}^2\Sigma_{11}(\text{BH}_b) + {}^3\Sigma_u^+(\text{H}_a\text{H}_b) - {}^1S_g(\text{B}) - {}^2S_g(\text{H}_a) - {}^2S_g(\text{H}_b)$
$H(1,6) = -\cos\varphi {}^2\Sigma_{12}(\text{BH}_b)$
$H(1,7) = -\sin\varphi {}^2\Sigma_{12}(\text{BH}_b)$
$H(1,8) = {}^2\Sigma_{12}(\text{BH}_a)$
$H(2,2) = \frac{2}{3}[{}^2\Sigma_{33}(\text{BH}_a) + \cos^2\varphi {}^2\Sigma_{33}(\text{BH}_b) + \sin^2\varphi {}^2\Pi_{22}(\text{BH}_b)] + \frac{1}{3}[{}^4\Sigma(\text{BH}_a) + \cos^2\varphi {}^4\Sigma(\text{BH}_b) + \sin^2\varphi {}^4\Pi(\text{BH}_b)] + {}^3\Sigma_u^+(\text{H}_a\text{H}_b) - {}^3P_u(\text{B}) - {}^2S_g(\text{H}_a) - {}^2S_g(\text{H}_b)$
$H(2,3) = \frac{\sqrt{2}}{3}\{[{}^2\Sigma_{33}(\text{BH}_a) - {}^4\Sigma(\text{BH}_a)] - [\cos^2\varphi {}^2\Sigma_{33}(\text{BH}_b) + \sin^2\varphi {}^2\Pi_{22}(\text{BH}_b)] + [\cos^2\varphi {}^4\Sigma(\text{BH}_b) + \sin^2\varphi {}^4\Pi(\text{BH}_b)]\}$
$H(2,4) = \frac{2}{3}\cos\varphi\sin\varphi[{}^2\Sigma_{33}(\text{BH}_b) - {}^2\Pi_{22}(\text{BH}_b)] + \frac{1}{3}\cos\varphi\sin\varphi[{}^4\Sigma(\text{BH}_b) - {}^4\Pi(\text{BH}_b)]$
$H(2,5) = -\frac{\sqrt{2}}{3}\cos\varphi\sin\varphi[{}^2\Sigma_{33}(\text{BH}_b) - {}^2\Pi_{22}(\text{BH}_b)] - [{}^4\Sigma(\text{BH}_b) - {}^4\Pi(\text{BH}_b)]$
$H(3,3) = \frac{1}{3}[{}^2\Sigma_{33}(\text{BH}_a) + \cos^2\varphi {}^2\Sigma_{33}(\text{BH}_b) + \sin^2\varphi {}^2\Pi_{22}(\text{BH}_b)] + \frac{2}{3}[{}^4\Sigma(\text{BH}_a) + \cos^2\varphi {}^4\Sigma(\text{BH}_b) + \sin^2\varphi {}^4\Pi(\text{BH}_b)] + {}^1\Sigma_g^+(\text{H}_a\text{H}_b) - {}^3P_u(\text{B}) - {}^2S_g(\text{H}_a) - {}^2S_g(\text{H}_b)$
$H(3,4) = -\frac{\sqrt{2}}{3}\cos\varphi\sin\varphi[{}^2\Sigma_{33}(\text{BH}_b) - {}^2\Pi_{22}(\text{BH}_b)] + [{}^4\Sigma(\text{BH}_b) - {}^4\Pi(\text{BH}_b)]$
$H(3,5) = \frac{1}{3}\cos\varphi\sin\varphi[{}^2\Sigma_{33}(\text{BH}_b) - {}^2\Pi_{22}(\text{BH}_b)] + 2[{}^4\Sigma(\text{BH}_b) - {}^4\Pi(\text{BH}_b)]$
$H(4,4) = \frac{\sqrt{2}}{3}[{}^2\Pi_{22}(\text{BH}_a) + \sin^2\varphi {}^2\Sigma_{33}(\text{BH}_b) + \cos^2\varphi {}^2\Pi_{22}(\text{BH}_b)] + \frac{1}{3}[{}^4\Pi(\text{BH}_a) + \sin^2\varphi {}^4\Sigma(\text{BH}_b) + \cos^2\varphi {}^4\Pi(\text{BH}_b)] + {}^3\Sigma_u^+(\text{H}_a\text{H}_b) - {}^3P_u(\text{B}) - {}^2S_g(\text{H}_a) - {}^2S_g(\text{H}_b)$
$H(4,5) = \frac{\sqrt{2}}{3}\{[{}^2\Pi_{22}(\text{BH}_a) - {}^4\Pi(\text{BH}_a)] - [\sin^2\varphi {}^2\Sigma_{33}(\text{BH}_b) + \cos^2\varphi {}^2\Pi_{22}(\text{BH}_b)] + [\sin^2\varphi {}^4\Sigma(\text{BH}_b) + \cos^2\varphi {}^4\Pi(\text{BH}_b)]\}$
$H(5,5) = \frac{1}{3}[{}^2\Pi_{22}(\text{BH}_a) + \sin^2\varphi {}^2\Sigma_{33}(\text{BH}_b) + \cos^2\varphi {}^2\Pi_{22}(\text{BH}_b)] + \frac{2}{3}[{}^4\Pi(\text{BH}_a) + \sin^2\varphi {}^4\Sigma(\text{BH}_b) + \cos^2\varphi {}^4\Pi(\text{BH}_b)] + {}^1\Sigma_g^+(\text{H}_a\text{H}_b) - {}^3P_u(\text{B}) - {}^2S_g(\text{H}_a) - {}^2S_g(\text{H}_b)$
$H(6,6) = {}^3\Sigma_0(\text{BH}_a) + \cos^2\varphi {}^2\Sigma_{22}(\text{BH}_b) + \sin^2\varphi {}^2\Pi_{11}(\text{BH}_b) + \frac{1}{2}[{}^2\Sigma_g(\text{H}_a\text{H}_b) + {}^2\Sigma_u(\text{H}_a\text{H}_b)] - {}^2P_u(\text{B}) - {}^2S_g(\text{H}_a) - {}^1S_g(\text{H}_b)$
$H(6,7) = \cos\varphi\sin\varphi[{}^2\Sigma_{22}(\text{BH}_b) - {}^2\Pi_{11}(\text{BH}_b)]$
$H(6,8) = \frac{1}{2}[{}^2\Sigma_g(\text{H}_a\text{H}_b) - {}^2\Sigma_u(\text{H}_a\text{H}_b)]$
$H(7,7) = {}^3\Pi_0(\text{BH}_a) + \sin^2\varphi {}^2\Sigma_{22}(\text{BH}_b) + \cos^2\varphi {}^2\Pi_{11}(\text{BH}_b) + \frac{1}{2}[{}^2\Sigma_g(\text{H}_a\text{H}_b) + {}^2\Sigma_u(\text{H}_a\text{H}_b)] - {}^2P_u(\text{B}) - {}^2S_g(\text{H}_a) - {}^1S_g(\text{H}_b)$
$H(7,9) = \frac{1}{2}[{}^2\Sigma_g(\text{H}_a\text{H}_b) - {}^2\Sigma_u(\text{H}_a\text{H}_b)]$
$H(8,8) = {}^2\Sigma_{22}(\text{BH}_a) + \cos^2\varphi {}^3\Sigma(\text{BH}_b) + \sin^2\varphi {}^3\Pi(\text{BH}_b) + \frac{1}{2}[{}^2\Sigma_g(\text{H}_a\text{H}_b) + {}^2\Sigma_u(\text{H}_a\text{H}_b)] - {}^2P_u(\text{B}) - {}^1S_g(\text{H}_a) - {}^2S_g(\text{H}_b)$
$H(8,9) = \cos\varphi\sin\varphi[{}^3\Sigma(\text{BH}_b) - {}^3\Pi(\text{BH}_b)]$
$H(9,9) = {}^2\Pi_{11}(\text{BH}_a) + \sin^2\varphi {}^3\Sigma(\text{BH}_b) + \cos^2\varphi {}^3\Pi(\text{BH}_b) + \frac{1}{2}[{}^2\Sigma_g(\text{H}_a\text{H}_b) + {}^2\Sigma_u(\text{H}_a\text{H}_b)] - {}^2P_u(\text{B}) - {}^1S_g(\text{H}_a) - {}^2S_g(\text{H}_b)$

^aThe symbol φ refers to the angle between B–H_a and B–H_b bonds in the molecule. Σ_{ij} and Π_{ij} refer to the elements of diabaticized sub-blocks corresponding to the BH⁺(²Σ) and BH⁺(²Π) fragments (see the text). See Tables I–V for other symbols. The potential-energy matrix is symmetrical and matrix elements not listed here as zero.

IX the cross section for all the products fall as the energy increases. This is typical of exothermic reaction without any energy barrier. We also note that the charge transfer process leading to the formation of H₂⁺ is the most efficient process at all energies. This clearly indicates that this system is a typical example of ion–molecule reaction where the nonadiabatic effect is quite important. There is a strong coupling between the lower surfaces in the entrance channel (corresponding to H₂ and H₂⁺) and as the reaction proceeds much of the wave packets go to the charge transfer state leading to B+H₂⁺. This also explains why we have obtained much smaller cross sections for the ground-state product BH⁺(X²Σ⁺) in comparison to that of the excited state one BH⁺(B²Σ⁺). This observation is further substantiated by the correlation properties of ground and excited surface as discussed earlier. The experimental support of the formation of BH⁺ in its excited state comes from the beam chemiluminescence experiment on this reaction by Ottinger and Reichmuth¹⁶ where a new emission was ascribed to this product. Finally, we have obtained significant cross section for the product BH(¹Σ⁺) also. Thus it appears that on this

triplet surface the reaction proceeds predominantly via two steps, that is the charge transfer leading the system to the excited state, and then reaction takes place mostly from the excited state and the ground state product comes out as a minor one. Finally, Figs. 5 and 6 show the product vibrational distribution for the various product species. We find that the formation of BH⁺ in the ground state is accompanied with significant vibrational excitation which is to be expected for this type of reaction. For all the product ions the vibrational cross sections in general decreases with the increase of energy.

Prior to the present study the QCT calculations have been reported on this reaction.¹⁴ However, a direct comparison of the QCT results with the present calculations is rendered difficult as the QCT calculations were carried out only on the lowest surface, ignoring thus the possible nonadiabatic effects in the reaction which has been found to be quite important here. In fact, the QCT studies predicted very small lifetimes of the collision complex in comparison to the experiment and one of the reasons for this discrepancy was conjectured to be the nonadiabatic transitions. As a result the

outcome of the present calculations are understandably in conflict with the QCT ones. For example, the QCT results have shown a fairly large cross sections for the ground-state $\text{BH}^+(^2\Sigma^+)$ product. On the contrary, the cross sections as found in the present study for $\text{BH}^+(^2\Sigma^+)$ is quite small in comparison to those of the excited states because of the profound nonadiabatic transitions in the entrance channel (see Table IX). Moreover, in the present study the ground state product $\text{BH}^+(^2\Sigma^+)$ is predicted to come out vibrationally hot (see Fig. 6) and the distribution of vibrational quantum numbers is qualitatively different from that found in the QCT calculations.

V. CONCLUSION

We have demonstrated in this paper the feasibility of the semiclassical wave packet methods in hyperspherical coordi-

nates to study the nonadiabatic processes occurring in three particle molecular dynamics, even in the system involving nine coupled electronic surfaces. Though we have not considered in the present study the present method could easily be extended to the spin-orbit coupled system also without much numerical effort as total computation scales only linearly with the number of surfaces. Compared to the traditional trajectory surface hopping scheme the present method offers the clear advantage that it takes into account the nonadiabatic effects in the molecular processes in a consistent manner; for example, we do not have to make any assumption of the transitions to be of Landau-Zener type and localized in space, and also we have no problem with arbitrary energy division among various degrees of freedom of the jump. We have utilized a recently proposed scheme to obtain the rotationally summed vibrational state distribution which

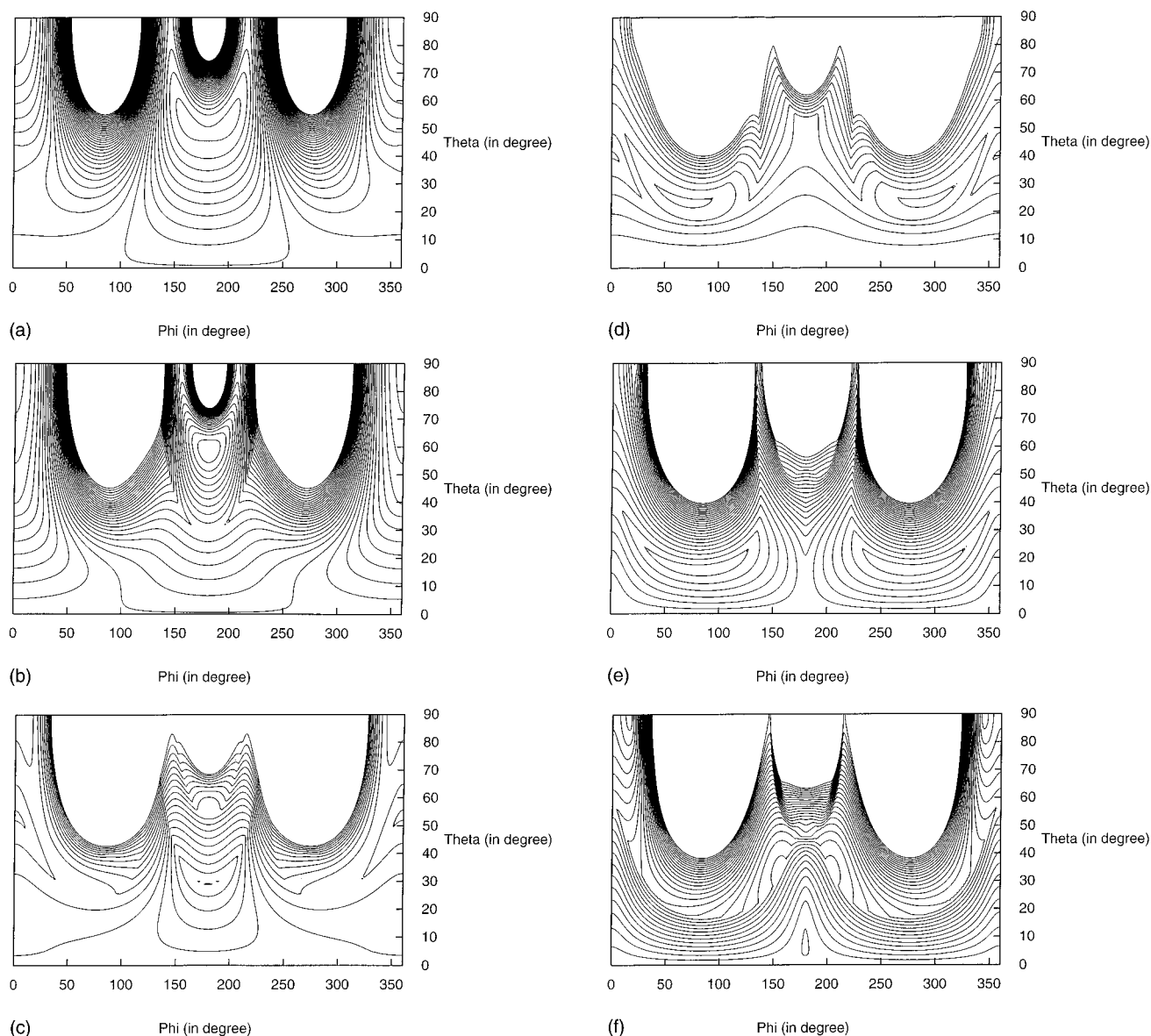


FIG. 2. Contour plot of the potential-energy surfaces near the classical turning point ($\rho=2 \text{ \AA}$). The contour spacing is $0.25 \hat{e}$ and starts from $-10 \hat{e}$ ($1 \hat{e} = 100 \text{ kJ/mol}$).

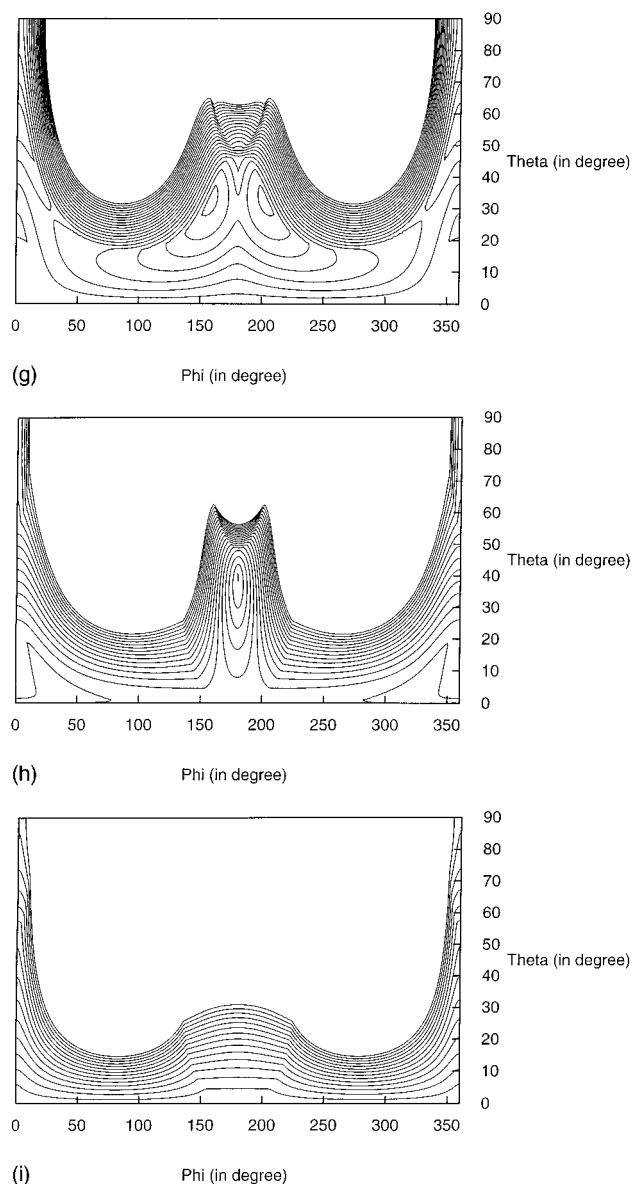


FIG. 2. (Continued).

avoids the problem associated with the coarse nature of the grid in the calculations. We have obtained the total cross sections for all channels (reactive as well as charge transfer) simultaneously by the grid summation method. Though the DIM potential-energy surfaces are admittedly approximate the present study has clearly shown that $\text{B}^+(\text{}^3P_u) + \text{H}_2$ reaction cannot be treated as a single surface problem. The scattering process appears to take place in two steps—charge transfer leading to the formation of H_2^+ which is an efficient one, followed by the rearrangement step leading to reaction. As a result we have obtained larger cross section for the BH^+ product in the excited states in comparison to that of the ground-state one. This has been substantiated by the beam chemiluminescence experimental study. Energy dependence of cross sections for various products show the typical behavior of exothermic reaction, and so also the product vibra-

tional distributions. To elucidate the mechanism further much experimental work is required for this reaction.

ACKNOWLEDGMENT

This research is supported by the Danish Natural Science Research Council.

APPENDIX

We present a brief review of the DIM method for triatomic molecules which we have utilized in the present study. More complete descriptions of the method can be found elsewhere.^{22–24} There are several equivalent formulations of this method and in this paper we essentially follow the scheme developed by Faist and Muckerman.^{12,13} In the nonrelativistic Born–Oppenheimer scheme the electronic eigenvalue equation is

$$\hat{\mathcal{H}}(R)|\chi_k(R)\rangle = \Omega_k(R)|\chi_k(R)\rangle, \quad (\text{A1})$$

where $\hat{\mathcal{H}}(R)$ is the electronic Hamiltonian operator which depends parametrically on the nuclear configuration R , $\Omega_k(R)$ is the electronic energy which is a function of R and $|\chi_k(R)\rangle$ is the eigenvector for the k th electronic state and this also depends parametrically on R . In the present work we have not considered the spin–orbit interaction, and therefore, the electronic eigenvalues are functions of three internuclear distances only (assuming three Euler angles which define the orientation of the triangle with respect to a space-fixed frame, are fixed at some convenient values), and thus here R represents only the internuclear distances. Since the general nuclear configuration of a triatomic molecule possesses only C_s symmetry we designate the energy levels with the symmetry species A' and A'' of the point group, though at some special configurations (belonging to $C_{\infty v}$ and C_{2v} point groups) energy levels could also be labeled by the appropriate symmetry species.

The derivation of the DIM Hamiltonian follows the basic ideas of “atoms in molecule” (AIM) originally due to Moffitt,²⁵ and the general expression is given as

$$\hat{\mathcal{H}}_{\text{DIM}} = \sum_p \sum_{q>p} \hat{\mathcal{H}}^{pq} - (N-2) \sum_p \hat{\mathcal{H}}^p, \quad (\text{A2})$$

where N is the number of atoms in molecule and $\hat{\mathcal{H}}^{pq}$ and $\hat{\mathcal{H}}^p$ are the Hamiltonian operator for the diatomic and atomic fragments of the molecule, respectively. Hence the total energy of the molecule within DIM framework is expressed as the sum of energies of all possible diatomic fragments minus the sum of atom energies as many times as necessary to correct for their multiple inclusion in the diatomic fragment energy sum. Thus for a general triatomic ABC we have

$$\hat{\mathcal{H}}_{\text{DIM}} = \hat{\mathcal{H}}^{AB} + \hat{\mathcal{H}}^{BC} + \hat{\mathcal{H}}^{AC} - \hat{\mathcal{H}}^A - \hat{\mathcal{H}}^B - \hat{\mathcal{H}}^C. \quad (\text{A3})$$

In the following we will drop the subscript DIM for the notational convenience. In a practical scheme of solving Eq. (1) we express $|\chi_k(R)\rangle$ in a general complete basis $\{|\Psi_i\rangle, i=1, M\}$ and thus we write in a matrix form

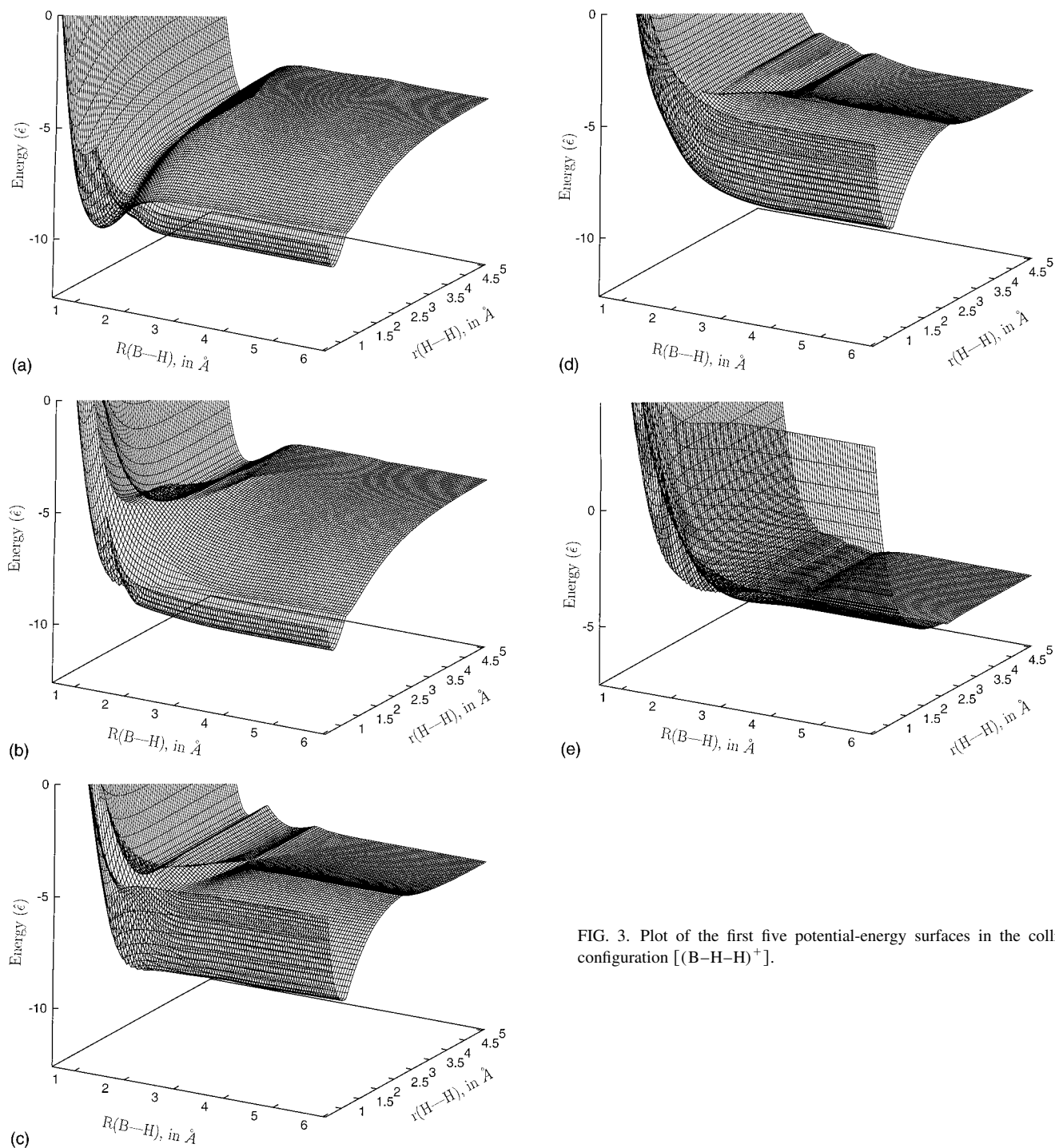


FIG. 3. Plot of the first five potential-energy surfaces in the collinear configuration $[(B-H-H)^+]$.

$$\chi = \Psi C, \quad (\text{A4})$$

where the coefficient matrix C completely determines the state $|\chi\rangle$. On putting Eq. (A4) into Eq. (A1) and premultiplying with $\langle\Psi|$ we obtain

$$HC = SC\Omega, \quad (\text{A5})$$

where $H = \langle\Psi|\hat{\mathcal{H}}|\Psi\rangle$ is the matrix representation of the Hamiltonian operator $\hat{\mathcal{H}}$ in the $|\Psi\rangle$ basis, $S = \langle\Psi|\Psi\rangle$, is the overlap matrix and Ω is the diagonal matrix containing the energy eigenvalues. In the following we continue the deriva-

tion assuming the basis to be complete, though in practice the basis is almost always truncated. The approximation involved with the truncated basis may be cast in the projection operator formulation which we will point out later. Since $\{|\chi_n\rangle\}$ is complete and orthonormal we can decompose unity into the sum of elementary projectors as

$$1 = \sum_n |\chi_n\rangle\langle\chi_n| = \chi\chi^\dagger. \quad (\text{A6})$$

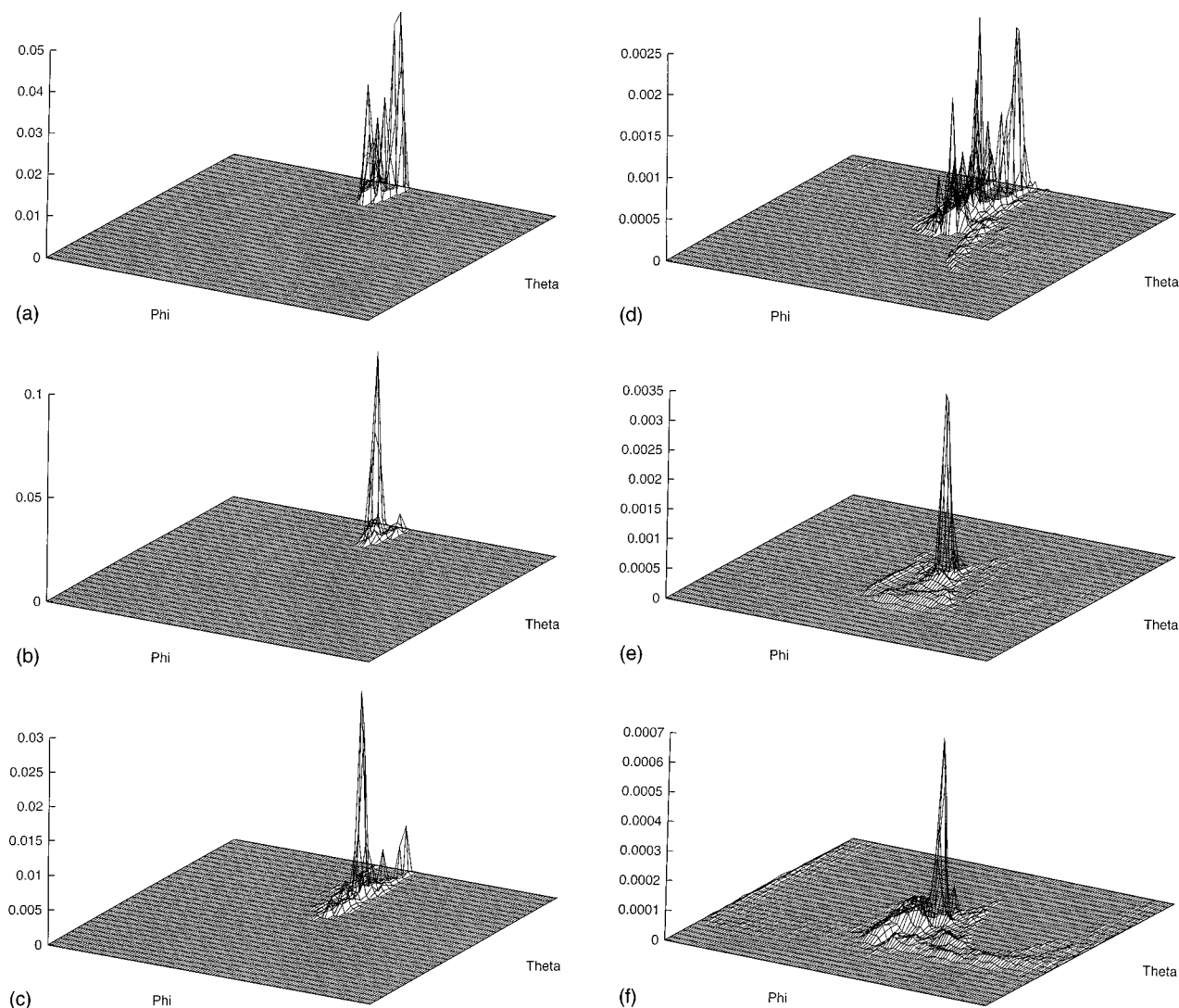


FIG. 4. The 2D wave packet on different electronic surfaces (A–I) at the end of collision at $1 \hat{\epsilon}$ energy ($1 \hat{\epsilon} = 100$ kJ/mol).

From Eqs. (A4) and (A6) we have

$$1 = \Psi C C^\dagger \Psi^\dagger = \Psi S^{-1} \Psi^\dagger, \quad (\text{A7})$$

where $C = S^{-1/2} U^\dagger$ with U^\dagger as unitary matrix independent of overlap. Using the elementary projector (A7) we can write the operation of $\hat{\mathcal{H}}$ on Ψ as

$$\hat{\mathcal{H}}\Psi = \Psi S^{-1} \Psi^\dagger \hat{\mathcal{H}}\Psi = \Psi S^{-1} H. \quad (\text{A8})$$

Now we introduce independent particle approximation, that is each polyatomic basis function (*pbf*) is composed of a linear combination of antisymmetrized products of one electron spin-orbitals and each of the spin-orbitals is centered on a specific nucleus according to the valence bond scheme. Thus we have

$$\Psi = \hat{A} \psi, \quad (\text{A9})$$

where ψ_i s are the primitive unsymmetrized *pbf* and \hat{A} is the usual antisymmetrization operator. The Hamiltonian opera-

tion on Ψ within DIM framework can be written as

$$\begin{aligned} \hat{\mathcal{H}}\Psi &= \hat{A} \hat{\mathcal{H}}\psi \\ &= \sum_p \sum_{q>p} \hat{A} \hat{\mathcal{H}}^{pq} \psi - (N-2) \sum_p \hat{A} \hat{\mathcal{H}}^p \psi. \end{aligned} \quad (\text{A10})$$

Following Ellison²⁶ we decompose \hat{A} into three different factors as

$$\hat{A} = \hat{A}_\nu^{(\nu)} \hat{A}_\nu \hat{A}_{(\nu)}, \quad (\text{A11})$$

where \hat{A}_ν antisymmetrizes only the electrons on ν fragment, $\hat{A}_{(\nu)}$ those not on ν fragment, and $\hat{A}_\nu^{(\nu)}$ completes the identity. In putting Eq. (A11) in Eq. (A10) we have

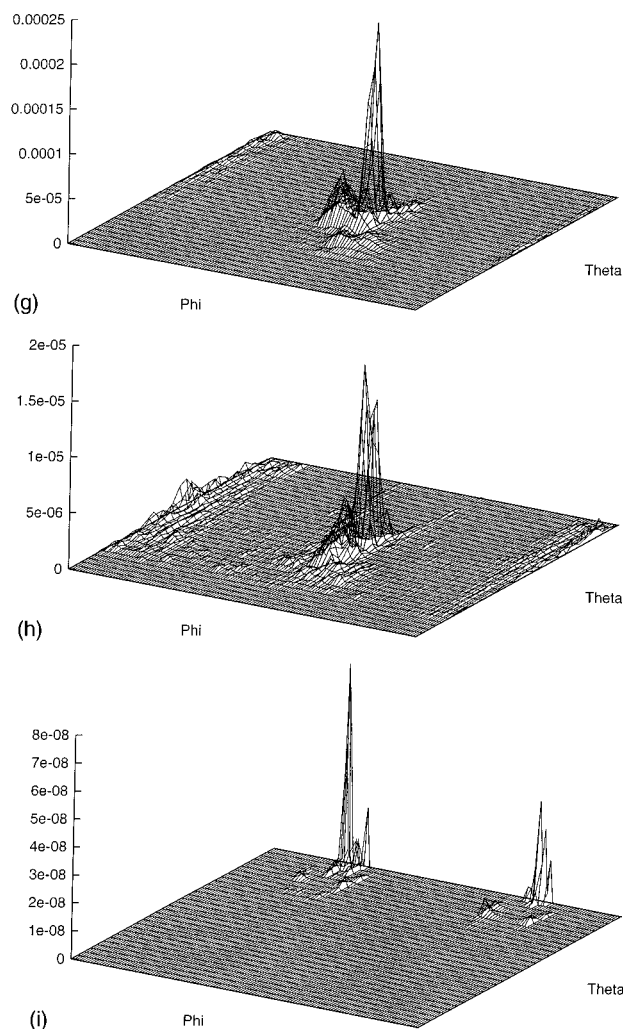


FIG. 4. (Continued.)

$$\begin{aligned}
 \hat{\mathcal{H}}\Psi &= \sum_p \sum_{q>p} \hat{A}_{pq}^{(pq)} \hat{A}_{pq} \hat{A}_{(pq)} \hat{\mathcal{H}}^{pq} \psi \\
 &\quad - (N-2) \sum_p \hat{A}_p^{(p)} \hat{A}_p \hat{A}_{(p)} \hat{\mathcal{H}}^p \psi \\
 &= \sum_p \sum_{q>p} \hat{A}_{pq}^{(pq)} \hat{\mathcal{H}}^{pq} \Phi^{pq} - (N-2) \sum_p \hat{A}_p^{(p)} \hat{\mathcal{H}}^p \Phi^{pq}.
 \end{aligned} \tag{A12}$$

with the following definition;

TABLE IX. Energy dependence of cross sections^a for various products.

Energy ^b	H ₂	BH ⁺ (X ² Σ ⁺)	BH(X ¹ Σ ⁺)	BH ⁺ (B ² Σ ⁺)
0.5	28.691	0.039	0.308	0.659
1.0	10.547	0.017	0.169	0.345
2.00	5.920	0.022	0.184	0.434
3.0	3.778	0.024	0.189	0.433
4.0	3.137	0.017	0.174	0.422
5.0	2.658	0.019	0.177	0.420
7.0	2.090	0.018	0.185	0.394

^aIn units of Å².

^bIn units of eV (1 eV = 100 kJ/mol).

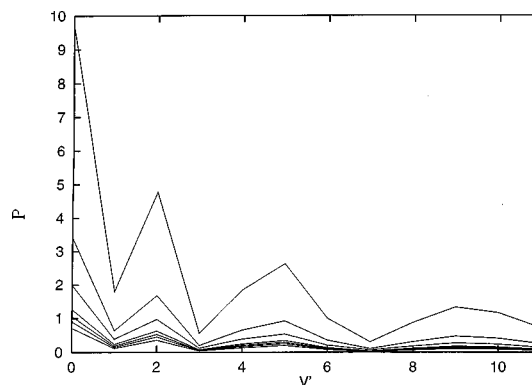


FIG. 5. Energy dependence of the vibrational distributions for H₂⁺. From top to bottom curves refer to 0.5 eV, 1 eV, 2 eV, 3 eV, 4 eV, 5 eV, and 7 eV energies, respectively, (1 eV = 100 kJ/mol).

$$\Phi^\nu \equiv \hat{A}_\nu \hat{A}_{(\nu)} \psi \equiv Y^\nu F_{(\nu)}. \tag{A13}$$

Here Y^ν is a row vector composed of antisymmetrized product of functions of only those electrons in the ν fragment and $F_{(\nu)}$ is the transformation matrix of antisymmetrized functions of the remaining electrons to complete the identity. Now if $\{\Psi_{ij}\}$ is complete in the polyatomic space, $\{Y_i^\nu\}$ is also complete in the ν fragment space spanned by the fragment Hamiltonian operator, $\hat{\mathcal{H}}^\nu$. Since $\hat{\mathcal{H}}^\nu$ operates only on the electrons associated with the ν fragment, $\{\Phi_i^\nu\}$ also spans the subspace of $\hat{\mathcal{H}}^\nu$. Thus we have the following resolution of identity [cf. Eq. (A7)]

$$1 = \Phi^\nu S_{\Phi^\nu}^{-1} \Phi^{\nu\dagger}, \tag{A14}$$

where

$$\begin{aligned}
 S_{\Phi^\nu} &= \Phi^{\nu\dagger} \Phi^\nu \\
 &= F_{(\nu)}^\dagger Y^{\nu\dagger} Y^\nu F_{(\nu)} \\
 &= F_{(\nu)}^\dagger S_{Y^\nu} F_{(\nu)}.
 \end{aligned} \tag{A15}$$

Now we examine the action of $\hat{\mathcal{H}}^\nu$ on Φ^ν as required in Eq. (A12) using the resolution of identity [cf. Eq. (A14)],

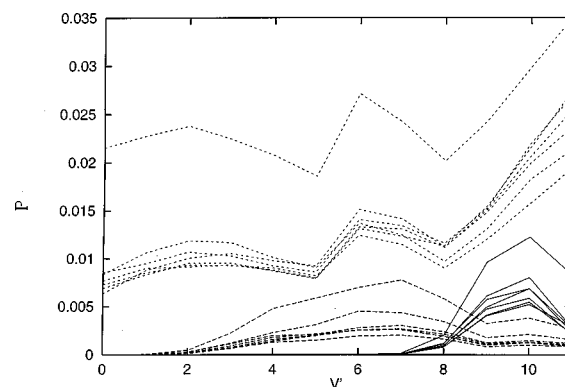


FIG. 6. Energy dependence of the vibrational distributions for BH⁺(X²Σ⁺) (full lines), BH(X¹Σ⁺) (broken lines), and BH⁺(B²Σ⁺) (dotted lines). For each species from top to bottom curves refer to 0.5 eV, 1 eV, 2 eV, 3 eV, 4 eV, 5 eV, and 7 eV energies, respectively, (1 eV = 100 kJ/mol).

$$\begin{aligned}\hat{\mathcal{H}}^{\nu}\Phi^{\nu} &= \Phi^{\nu}S_{\Phi^{\nu}}^{-1}\Phi^{\nu\dagger}\hat{\mathcal{H}}^{\nu}\Phi^{\nu} \\ &= \Phi^{\nu}S_{\Phi^{\nu}}^{-1}H^{\nu},\end{aligned}\quad (\text{A16})$$

where H^{ν} is given as follows [using Eq. (A13)].

$$\begin{aligned}H^{\nu} &= \Phi^{\nu\dagger}\hat{\mathcal{H}}^{\nu}\Phi^{\nu} \\ &= F_{(\nu)}^{\dagger}\Upsilon^{\nu\dagger}\hat{\mathcal{H}}^{\nu}\Upsilon^{\nu}F_{(\nu)} \\ &= F_{(\nu)}^{\dagger}H_{\Upsilon^{\nu}}F_{(\nu)}.\end{aligned}\quad (\text{A17})$$

Here in Eq. (A17) $H_{\Upsilon^{\nu}}$ is the Hamiltonian matrix for the pure ν fragment and the effect of integration implied by the $F_{(\nu)}$ matrix is to couple the appropriate elements of $H_{\Upsilon^{\nu}}$ for use in the polyatomic Hamiltonian. Now we substitute Eq. (A16) into Eq. (A12) to obtain

$$\begin{aligned}\hat{\mathcal{H}}\Psi &= \sum_p \sum_{q>p} A_{pq}^{(pq)}\hat{\mathcal{H}}^{pq}\Phi^{pq} - (N-2)\sum_p A_p^{(p)}\hat{\mathcal{H}}^p\Phi^p \\ &= \sum_p \sum_{q>p} A_{pq}^{(pq)}\Phi^{pq}S_{\Phi^{pq}}^{-1}H^{pq} - (N-2) \\ &\quad \times \sum_p A_p^{(p)}\Phi^pS_{\Phi^p}^{-1}H^p \\ &= \sum_p \sum_{q>p} \Psi S_{\Phi^{pq}}^{-1}H^{pq} - (N-2)\sum_p \Psi S_{\Phi^p}^{-1}H^p,\end{aligned}\quad (\text{A18})$$

where the last identity is obtained using Eqs. (A9), (A11), and (A13). Multiplying on the left by Ψ^{\dagger} on both sides we obtain

$$\begin{aligned}\Psi^{\dagger}\hat{\mathcal{H}}\Psi &= \sum_p \sum_{q>p} \Psi^{\dagger}\Psi S_{\Phi^{pq}}^{-1}H^{pq} - (N-2) \\ &\quad \times \sum_p \Psi^{\dagger}\Psi S_{\Phi^p}^{-1}H^p,\end{aligned}\quad (\text{A19})$$

$$H = \sum_p \sum_{q>p} SS_{\Phi^{pq}}^{-1}H^{pq} - (N-2)\sum_p SS_{\Phi^p}^{-1}H^p.\quad (\text{A20})$$

Directional orbitals

The orientation chosen in the pbf would not be optimum for all fragment diatomics if the latter contains the orbitals having the directional character, and hence the fragment matrix $H_{\Upsilon^{\nu}}$ in Eq. (A17) will reflect this deficiency. In order to remedy this problem we define a transformation matrix Q^{pq} which relates the old basis $\{Y_i^{pq}\}$ to a new aligned basis $\{\bar{Y}_i^{pq}\}$ in such a way that in this new set all directional orbitals are properly aligned:

$$\Upsilon^{pq} = \bar{Y}^{pq}Q^{pq}.\quad (\text{A21})$$

The Hamiltonian matrix for the diatomic fragment thus takes the form [cf. Eq. (A17)]

$$\begin{aligned}H_{\Upsilon^{pq}} &= \Upsilon^{pq\dagger}\hat{\mathcal{H}}^{pq}\Upsilon^{pq} \\ &= Q^{pq\dagger}\bar{Y}^{pq\dagger}\hat{\mathcal{H}}^{pq}\bar{Y}^{pq}Q^{pq} \\ &= Q^{pq\dagger}\bar{H}_{\Psi^{pq}}Q^{pq}.\end{aligned}\quad (\text{A22})$$

Thus the final DIM equation is

$$H_{\text{DIM}} = \sum_p \sum_{p>q} \bar{H}^{pq} - (N-2)\sum_p \bar{H}^p,\quad (\text{A23})$$

where

$$\begin{aligned}\bar{H}^{pq} &= SS_{\Phi^{pq}}^{-1}F_{(pq)}^{\dagger}Q_{pq}^{\dagger}\bar{H}_{\Psi^{pq}}Q_{pq}F_{(pq)}, \\ \bar{H}^p &= SS_{\Phi^p}^{-1}F_{(p)}^{\dagger}\bar{H}_{\Psi^p}F_{(p)}.\end{aligned}\quad (\text{A24})$$

The fundamental DIM approximations are hidden in the resolution of identity [cf. Eqs. (A7) and (A14)] which is true only for the complete basis limit. The complete basis is almost always impractical and its implication has been found to be the fact that the right hand side of Eq. (A24) becomes non-Hermitian. The origin of non-Hermitian character of Eq. (A24) has been discussed in the literature.^{12,13} This problem can be avoided in the practical approach of DIM. We first introduce the so-called ZOOA (zero overlap of atomic orbitals) approximation under which we have $S = S_{\Phi^{\nu}}$ for all the fragments. Thus Eq. (A24) reduces to

$$\begin{aligned}\bar{H}^{pq} &= F_{(pq)}^{\dagger}Q_{pq}^{\dagger}\bar{H}_{\Psi^{pq}}Q_{pq}F_{(pq)}, \\ \bar{H}^p &= F_{(p)}^{\dagger}\bar{H}_{\Psi^p}F_{(p)}.\end{aligned}\quad (\text{A25})$$

The right-hand side of Eq. (A25) is now clearly Hermitian term by term. Further we follow the semiempirical approach to DIM wherein all the diatomic and atomic fragment information required in Eq. (A25) is obtained empirically either from experimental or other theoretical sources. This formally completes the DIM scheme followed in this paper for obtaining multidimensional potential-energy surfaces for $(\text{BH}_2)^+$ molecular system. The construction of $F_{(\nu)}$ matrix has been explained in Ref. 13 which, under ZOOA approximation is given as

$$F_{(\nu)} = C_{\nu}^{\dagger}G_{(\nu)}.\quad (\text{A26})$$

The construction of the transformation matrices C_{ν} and $G_{(\nu)}$ will be discussed in the text.

- ¹G. D. Billing and N. Marković, *Chem. Phys.* **209**, 377 (1996).
- ²F. Aguillon, M. Sizun, V. Sidis, G. D. Billing, and N. Marković, *J. Chem. Phys.* **104**, 4530 (1996).
- ³M. Sizun, F. Aguillon, V. Sidis, V. Zenevich, G. D. Billing, and N. Marković, *Chem. Phys.* **209**, 327 (1996).
- ⁴N. Marković and G. D. Billing, *Chem. Phys.* **191**, 247 (1995).
- ⁵G. D. Billing and N. Marković, *J. Chem. Phys.* **99**, 2674 (1993).
- ⁶N. Marković and G. D. Billing, *Chem. Phys. Lett.* **195**, 53 (1992).
- ⁷N. Marković and G. D. Billing, *Chem. Phys.* **173**, 385 (1993).
- ⁸N. Marković and G. D. Billing, *Chem. Phys. Lett.* **248**, 420 (1996).
- ⁹J. T. Muckerman, R. D. Gilbert, and G. D. Billing, *J. Chem. Phys.* **88**, 4779 (1988).
- ¹⁰G. D. Billing and J. T. Muckerman, *J. Chem. Phys.* **91**, 6830 (1989).
- ¹¹G. D. Billing, *Encyclopedia of Computational Chemistry*, edited by H. F. Schaefer III (in press).

- ¹²M. B. Faist and J. T. Muckerman, *J. Chem. Phys.* **71**, 225 (1979).
¹³M. B. Faist and J. T. Muckerman, *J. Chem. Phys.* **71**, 233 (1979).
¹⁴V. Klimo, J. Tiño, and J. Urban, *Chem. Phys.* **137**, 33 (1989).
¹⁵B. Friedrich and Z. Herman, *Chem. Phys.* **69**, 433 (1982).
¹⁶Ch. Ottinger and J. Reichmuth, *J. Chem. Phys.* **74**, 928 (1981).
¹⁷B. R. Johnson, *J. Chem. Phys.* **79**, 1906 (1983).
¹⁸B. R. Johnson, *J. Chem. Phys.* **79**, 1916 (1983).
¹⁹C. E. Moore, Atomic Energy Levels, NBS Circular 467 (U.S. G-PO, Washington, DC, 1949).
²⁰F. Schneider, L. Zülicke, R. Polák, and J. Vojtík, *Chem. Phys.* **84**, 217 (1982).
²¹M. Baer, *Adv. Chem. Phys.* **82**, 187 (1992).
²²J. C. Tully, *J. Chem. Phys.* **58**, 1396 (1973).
²³P. J. Kuntz, in *Atom-Molecule Collision Theory*, edited by R. B. Bernstein (Plenum, New York, 1979).
²⁴F. A. Gianturco and F. Schneider, *Adv. Chem. Phys.* **82**, 135 (1992).
²⁵W. Moffit, *Proc. R. Soc. (London) Ser. A* **210**, 245 (1951).
²⁶F. O. Ellison, *J. Am. Chem. Soc.* **85**, 3540 (1963).